Available Online: 21 September 2026 DOI: 10.54254/3049-5458/2026.37192

Cell-type composition, cognitive performance, and neuropathologic correlates in aging and dementia

Banruo (Julie) Wang

Pepperdine University, Los Angeles, USA

banruow@gmail.com

Abstract. Alzheimer's disease and related dementias are increasingly understood as multicellular disorders in which neurons, glia, and vascular-associated cells may contribute differently to cognitive status and neuropathologic burden. This manuscript summarizes figure-level findings from a postmortem aging and dementia dataset that measured cortical cell-type proportions and tested their associations with dementia diagnosis, cognitive scores, time from last assessment, and common neuropathologies. Across the figures, dementia status was associated with higher astrocyte, L4 Intratelencephalic (IT), and microglia/Perivascular Macrophage (PVM) proportions, whereas no-dementia cases showed higher L2/3 IT and oligodendrocyte proportions. Better cognitive performance on the Cognitive Abilities Screening Instrument (CASI) and Mini-Mental State Examination (MMSE) was generally associated with higher proportions of selected excitatory neuronal subtypes and lower proportions of inflammatory or vascular-associated glial compartments. Neuropathologic measures, including Alzheimer's disease classification, Braak stage, CERAD score, Cerebral Amyloid Angiopathy (CAA), Lewy body disease, microinfarcts, atherosclerosis, arteriolosclerosis, and Limbic-predominant Age-related TDP-43 Encephalopathy (LATE), were associated with distinct cell-type profiles. These findings support the interpretation that dementia-related cellular changes are not limited to neuronal loss, but involve coordinated shifts in excitatory neurons, inhibitory interneurons, oligodendroglia, astrocytes, microglia, and vascular-associated populations. Because the current report is based on provided figures rather than the raw dataset, conclusions should be interpreted as exploratory and descriptive.

Keywords: dementia, Alzheimer's disease, single-nucleus RNA sequencing, cell-type proportions, neuropathology, cognition

1. Introduction

Dementia in late life is rarely explained by a single pathologic process. Alzheimer's disease neuropathologic change, Lewy body disease, vascular brain injury, LATE, and other age-associated lesions often co-occur and jointly influence cognitive decline [1-4]. Clinical-pathologic cohort studies such as the Religious Orders Study and the Rush Memory and Aging Project have been especially important because they connect longitudinal cognitive evaluation with brain donation and detailed neuropathologic assessment [5]. This design allows researchers to ask whether cognitive impairment is associated not only with lesions, but also with changes in the cellular composition of the aging human brain.

Copyright: © 2026 by the authors. Submitted for possible open access publication under the terms and conditions of the Creative Commons Attribution (CC BY) license (https://creativecommons.org/licenses/by/4.0/).

Single-nucleus and single-cell transcriptomic approaches have made it possible to classify major and rare brain cell populations in postmortem tissue and to test whether specific neuronal, glial, immune, or vascular-associated populations vary by disease state [6, 7]. Prior work using human Alzheimer's disease brain tissue has shown that pathology is accompanied by cell-type-specific molecular changes across excitatory neurons, inhibitory neurons, oligodendrocytes, astrocytes, microglia, and endothelial or vascular-associated cells [8-13]. These findings suggest that dementia is better conceptualized as a multicellular network disorder than as a purely neuronal disease.

One important question in Alzheimer's disease research is why some brain cell populations appear more vulnerable than others. Excitatory neurons, especially specific cortical projection neuron subtypes, have been shown to display selective molecular vulnerability in Alzheimer's disease, suggesting that cognitive decline may be linked to disruption of particular cortical circuits rather than uniform neuronal loss [10, 11]. At the same time, non-neuronal populations may actively shape the disease environment. Microglia and astrocytes can shift into disease-associated states during aging and neurodegeneration, reflecting immune activation, inflammatory signaling, synaptic remodeling, and responses to amyloid or tau pathology [13-15]. Therefore, examining both neuronal and glial cell percentages may help clarify whether dementia-related changes are driven by neuronal vulnerability, reactive glial responses, or a combination of both.

In addition to Alzheimer's disease pathology, vascular and mixed pathologies are important to consider because many older adults with dementia have more than one neuropathologic process at autopsy. Vascular brain injury, microinfarcts, arteriolosclerosis, cerebral amyloid angiopathy, Lewy body disease, and LATE can each contribute to cognitive impairment and may lower the threshold for clinically apparent dementia when they occur alongside Alzheimer's disease neuropathologic change [1, 2, 16, 17]. For this reason, studying cell-type percentages in relation to both clinical measures and neuropathologic variables may provide a more complete view of how multiple disease processes are reflected in the aging brain.

The provided figures summarize analyses of cell-type percentages in relation to clinical diagnosis, cognitive performance, and neuropathologic variables. The cell-type labels include excitatory neuronal subtypes such as L2/3 IT, L4 IT, L5 IT, L5/6 Near-Projecting (NP), L6 Corticothalamic (CT), and L6b; inhibitory populations such as Pvalb, Lamp5, Pax6, Vip, Sst Chodl, and chandelier cells; glial populations including astrocytes, oligodendrocytes, Oligodendrocyte Precursor Cells (OPCs), and microglia/PVM; and vascular-associated populations such as Vascular Leptomeningeal Cells (VLMCs) and endothelial cells. These cell categories are relevant because prior work has identified disease-associated astrocyte and microglial states, selective neuronal vulnerability, oligodendrocyte and myelin-related changes, and vascular-cell dysregulation in Alzheimer's disease and related dementias [9, 10, 14, 15, 18]. The figures also include common clinical and neuropathologic measures, including CASI, MMSE, Braak stage, CERAD score, CAA, Lewy body disease, microinfarcts, atherosclerosis, arteriolosclerosis, LATE stage, and RNA Integrity Number (RIN).

2. Methods

Data were obtained from the Seattle Alzheimer's Disease Brain Cell Atlas (SEA-AD) [19], a publicly available resource hosted through the Allen Institute Brain Map portal. The SEA-AD dataset includes donor-level demographic, clinical, cognitive, neuropathologic, and molecular data from postmortem human brain tissue. The present analysis used donor metadata and cell-type count information from two brain regions included in the SEA-AD resource: the Prefrontal Cortex (PFC; A9) and Middle Temporal Gyrus (MTG). Data were

accessed through the SEA-AD public portal at https://brain-map.org/consortia/sea-ad and the SEA-AD data page at https://brain-map.org/consortia/sea-ad/our-data.

The donor metadata were downloaded from SEA-AD and organized in Microsoft Excel with the corresponding PFC and MTG cell-type count data. Each row represented an individual donor, and the spreadsheet included demographic variables, clinical and cognitive measures, neuropathologic variables, RNA Integrity Number (RIN), and cell-type measurements. Variables used in the analysis included age at death, sex, education level, dementia diagnosis, last CASI score, last MMSE score, months between cognitive testing and death, Braak stage, CERAD score, cerebral amyloid angiopathy, Lewy body disease, microinfarcts, atherosclerosis, arteriolosclerosis, LATE stage, and RIN.

Cell-type abundance was calculated as a percentage for each donor. For each cell type, the number of cells assigned to that cell type was divided by the total number of cells for the same donor and multiplied by 100. This calculation was performed separately for each donor and cell type using the formula: cell-type percentage = (number of cells in a specific cell type / total number of cells per donor) × 100. The calculated percentages were then used as the main outcome variables in the analysis. After the Excel spreadsheet was created, the data were imported into Python and analyzed in Jupyter Notebook. Data preparation included checking column names, confirming donor-level matching across metadata and cell-type data, reviewing missing values, and making sure categorical variables were coded consistently. Continuous variables, including age at death, CASI score, MMSE score, months between cognitive testing and death, RIN, and cell-type percentages, were treated as numeric variables. Categorical variables, including dementia status, sex, education level, Braak stage, CERAD score, vascular pathology measures, Lewy body disease, LATE stage, and RIN group, were treated as grouping variables.

Exploratory analyses were performed to examine whether cell-type percentages differed by demographic, cognitive, neuropathologic, and technical-quality variables. Continuous predictors were analyzed using correlation or regression-based approaches and visualized with scatterplots. Two-group categorical variables, such as dementia status, sex, microinfarct status, and high versus low RIN, were compared using group-comparison analyses. Categorical variables with more than two levels, such as education, Braak stage, CERAD score, atherosclerosis, arteriolosclerosis, Lewy body disease, and LATE stage, were evaluated using analysis of variance or equivalent group-comparison procedures. Graphs were generated in Python to display the associations between each selected variable and donor-level cell-type percentages.

Because this study used publicly available donor-level data and calculated cell-type percentages, all findings were interpreted as exploratory associations rather than causal relationships. Cell-type percentages were also treated as compositional measures, meaning that an apparent increase in one cell type may partly reflect a relative decrease in another cell type. Therefore, the results were interpreted cautiously and used to identify cell populations that may warrant further analysis with adjusted statistical models.

3. Results

Broad demographic and diagnostic characteristics were first examined for associations with differences in cellular composition. Because aging is the central risk context for late-life cognitive decline, age at death was examined in relation to the overall percentage of cells, and a positive association was found, suggesting that cellular composition varied systematically across the age range of the cohort (Figure A1A). Participants with dementia were then compared with those without dementia to test whether clinical diagnosis was accompanied by shifts in specific cell populations. Dementia cases showed higher astrocyte and L4 IT proportions, whereas participants without dementia showed higher L2/3 IT and oligodendrocyte proportions (Figure A1B-E).

Dementia was also associated with higher microglia-PVM proportions, supporting the idea that cognitive impairment is accompanied by both inflammatory and neuronal-cell-type changes (Figure A1F). Because demographic variables may shape brain aging trajectories, education and sex were additionally examined. Pvalb proportions varied across education groups, and L6b proportions differed by sex, indicating that non-disease characteristics may also contribute to observed cellular heterogeneity (Figure A1G-H).

After establishing that dementia status was associated with cellular differences, the next analysis examined whether cell-type proportions tracked with cognitive performance across individuals. To address this question, the last CASI score was examined as a continuous measure of global cognition. Higher CASI scores were associated with lower astrocyte, microglia-PVM, and VLMC proportions, suggesting that poorer cognitive status may be linked to increased glial, immune, and vascular-associated cellular signals (Figure A2A, 2F-G). In contrast, higher CASI scores were associated with higher L2/3 IT, L6 CT, L5 ET, and Sst Chodl proportions, indicating that better cognition may be related to preservation or enrichment of selected excitatory and inhibitory neuronal populations (Figure A2B, 2D-E, 2H). L4 IT showed a negative association with CASI score, suggesting that not all excitatory neuron subtypes followed the same cognitive pattern (Figure A2C).

Similar cognitive associations were then evaluated using MMSE, and the potential influence of the timing of the final cognitive assessment was also examined. A longer interval between last CASI assessment and death was positively associated with L5 IT proportions, indicating that proximity of cognitive testing to death may influence how cellular findings relate to clinical status (Figure A3A). Using last MMSE score, higher cognition was associated with higher L2/3 IT, L5/6 NP, and Sst Chodl proportions, reinforcing the pattern that some neuronal populations are more abundant among participants with better cognitive performance (Figure A3B-C, 3G). In contrast, Lamp5, Pax6, and Vip proportions were negatively associated with MMSE score, showing that inhibitory neuron subclasses may relate to cognition in subtype-specific rather than uniform directions (Figure A3D-F).

Because clinical dementia often reflects multiple neuropathologic processes, the next analysis examined whether cell-type proportions varied with Alzheimer's disease and vascular pathology markers. A longer interval between last MMSE and death was associated with lower oligodendrocyte proportions, again emphasizing that clinical-pathologic timing may matter (Figure A4A). Alzheimer's disease neuropathologic classification was associated with L5/6 NP proportions, and Braak stage was associated with L2/3 IT and Vip proportions, suggesting that tau-related disease progression may be reflected in both excitatory and inhibitory neuronal populations (Figure A4B-D). CERAD neuritic plaque score was associated with L2/3 IT, OPC, and Sst Chodl proportions, indicating that amyloid-related pathology may also correspond to changes across neuronal and glial-lineage compartments (Figure A4E-G). Finally, cerebral amyloid angiopathy severity was associated with Lamp5 Lhx6 and RIN, raising the possibility that vascular amyloid burden and tissue-quality measures should be considered when interpreting cellular composition (Figure A4H-I).

Non-Alzheimer's pathologies were also examined for distinct cellular signatures. Highest Lewy body disease category was associated with chandelier cell proportions, suggesting that synaptic inhibitory circuitry may be sensitive to Lewy body-related disease burden (Figure A5A). Participants with no microinfarcts were then compared with those with at least one microinfarct not observed grossly. Microinfarcts were associated with lower astrocyte and microglia proportions but higher L6b and Sst Chodl proportions, indicating that microscopic vascular injury may correspond to a cellular pattern that differs from the dementia and CASI-related glial increases observed earlier (Figure A5B-E).

Finally, additional vascular, LATE, and technical-quality variables were examined to determine whether the observed cellular patterns were specific to clinical disease or also influenced by tissue and vascular context. Atherosclerosis severity was associated with L6b.1 and Vip.1 proportions, while arteriolosclerosis severity

was associated with L6 IT Car3 proportions, supporting a relationship between vascular disease burden and selected neuronal subtypes (Figure A6A-C). LATE stage was associated with L5/6 NP.1 and oligodendrocyte.1 proportions, suggesting that TDP-43-related pathology may have its own cellular correlates (Figure A6D-E). Because RNA integrity can influence single-nucleus measurements, high- and low-RIN groups were compared, revealing differences in endothelial, L2/3 IT, oligodendrocyte, and VLMC proportions (Figure A6F-I). These RIN-related findings indicate that technical quality is not merely a background variable but a factor that should be considered when interpreting disease-associated cell-type differences.

4. Discussion

The provided figures show a consistent pattern in which cognitive impairment and neuropathologic burden are associated with shifts across multiple brain cell classes. Dementia status was linked to higher astrocyte and microglia/PVM proportions and lower L2/3 IT and oligodendrocyte proportions. This pattern is compatible with a model in which dementia involves both neuronal vulnerability and glial or immune activation. Recent work has shown that AD-related cellular changes are distributed across neuronal, glial, immune, and vascular-associated compartments rather than being limited to neurons alone [10, 11]. The higher astrocyte and microglia/PVM proportions among dementia cases may reflect reactive gliosis, inflammatory recruitment, relative neuronal depletion, or a combination of these mechanisms. Microglial and astrocytic disease-associated states have been described in aging and Alzheimer's disease, supporting the interpretation that glial changes may reflect active responses to neurodegeneration rather than passive background variation [14, 20, 21]. The lower oligodendrocyte proportions in dementia and with longer time from last MMSE to death may indicate vulnerability of myelinating cells or altered white matter-related support in advanced disease. This interpretation is consistent with recent studies showing that oligodendrocyte and myelin-related dysfunction may contribute to Alzheimer's disease progression and cognitive impairment [18, 22].

The cognitive-score results highlight the importance of excitatory neuronal subtypes. Higher CASI and MMSE scores were repeatedly associated with higher L2/3 IT proportions, and higher cognition was also associated with L6 CT, L5 ET, L5/6 NP, and Sst Chodl proportions in selected panels. L2/3 IT neurons are cortico-cortical projection neurons that may be particularly relevant to distributed cognitive networks. Their positive association with cognitive scores and their variation by Braak and CERAD measures suggest that superficial-layer excitatory neurons may be an informative cellular marker of cognitive resilience or vulnerability. Prior single-nucleus studies similarly suggest that specific excitatory neuronal populations show selective vulnerability in Alzheimer's disease, which may help explain why cognitive decline is linked to disruption of particular cortical circuits rather than uniform neuronal loss [10]. However, because the figures present percentages, apparent increases or decreases could reflect true biological changes or relative shifts caused by changes in other cell populations. This is important because cell-type percentage data are compositional, meaning that the measured proportion of one population can change when another population expands or contracts [23].

The inhibitory neuron results were more heterogeneous. Pvalb varied by education; Lamp5, Pax6, and Vip were negatively associated with MMSE; Sst Chodl was positively associated with both CASI and MMSE; and chandelier cells varied by Lewy body disease category. These findings suggest that inhibitory interneuron subtypes may not respond uniformly to dementia or neuropathology. Interneuron subtypes differ in laminar distribution, circuit function, and molecular identity, so disease-associated changes in one inhibitory population should not be generalized to all inhibitory neurons. This interpretation is consistent with

transcriptomic classification studies showing that cortical GABAergic neurons are highly diverse and contain many molecularly distinct subtypes [24].

The neuropathology panels support the view that different disease processes may have distinct cellular signatures. Alzheimer's disease-related variables, including Braak stage and CERAD score, were associated with excitatory neuronal and interneuron proportions. CAA was associated with Lamp5 Lhx6 and RIN, while vascular pathologies such as microinfarcts, atherosclerosis, and arteriolosclerosis were associated with glial, excitatory neuronal, and inhibitory neuronal subtypes. Vascular and blood-brain barrier dysfunction are increasingly recognized as contributors to cognitive impairment and may interact with neurodegenerative pathology in aging brains [25, 26]. LATE stage was associated with L5/6 NP and oligodendrocyte proportions. These associations are clinically important because mixed pathologies are common in older adults, and a single diagnostic label may obscure distinct cellular mechanisms. The vascular-related findings are also consistent with evidence that APOE4 and vascular dysfunction can contribute to cognitive decline independently of classical amyloid and tau measures [27].

These findings also fit with current Alzheimer's disease frameworks that emphasize biological staging and neuropathologic burden rather than relying only on clinical diagnosis. Alzheimer's disease is defined by characteristic amyloid-β plaques, tau neurofibrillary tangles, and related neuropathologic changes, but the relationship between pathology and clinical symptoms is not always one-to-one [28]. Recent diagnostic and staging criteria further emphasize that AD can be understood biologically, while clinical dementia may still reflect the combined influence of AD pathology, vascular disease, Lewy body disease, LATE, and other age-related processes [29]. Therefore, the cell-type associations shown in the figures may be most meaningful when interpreted as part of a broader clinicopathologic framework rather than as markers of a single disease pathway.

The RIN findings are especially important. High versus low RIN was associated with endothelial, L2/3 IT, oligodendrocyte, and VLMC proportions. This does not mean that RIN biologically causes these differences; rather, it indicates that tissue quality or technical processing may influence measured cell-type proportions. Recent postmortem brain RNA studies show that RIN and postmortem interval can affect sequencing quality metrics and gene-expression estimates, which supports treating RIN as a key technical covariate in transcriptomic analyses [30, 31]. Future analyses should adjust for RIN and related technical variables to distinguish biological differences from potential measurement artifacts.

Several limitations should be noted. First, this manuscript was prepared from figures only and did not have access to the raw data, full model specifications, covariates, or multiple-comparison correction procedures. Second, the reported associations are observational and cannot establish causality. Third, cell-type percentages are compositional data; an apparent increase in one cell type may partly reflect decreases in other cell types. Fourth, some categories had small sample sizes, which may reduce precision and increase sensitivity to outliers. Finally, the figures do not indicate whether analyses adjusted for age, sex, education, postmortem interval, RIN, batch, or comorbid pathology, all of which are relevant in postmortem human brain research.

5. Conclusion

Overall, the figures suggest that dementia and age-related neuropathologies are associated with coordinated changes in neurons, glia, immune cells, and vascular-associated cells. The most consistent cognitive pattern involved better performance with higher selected excitatory neuronal proportions and lower astrocyte, microglia/PVM, and VLMC proportions. The findings support further adjusted, participant-level analysis to

test whether specific cell-type proportions independently predict cognition after accounting for mixed pathology and technical quality.

References

[1] Gorelick, P. B., Scuteri, A., Black, S. E., DeCarli, C., Greenberg, S. M., Iadecola, C., Launer, L. J., Laurent, S., Lopez, O. L., Nyenhuis, D., Petersen, R. C., Schneider, J. A., Tzourio, C., Arnett, D. K., Bennett, D. A., Chui, H. C., Higashida, R. T., Lindquist, R., Nilsson, P. M., … Seshadri, S. (2011). Vascular contributions to cognitive impairment and dementia: A statement for healthcare professionals from the American Heart Association/American Stroke Association. *Stroke, 42*(9), 2672–2713. https://doi.org/10.1161/STR.0b013e3182299496

[2] Kapasi, A., DeCarli, C., & Schneider, J. A. (2017). Impact of multiple pathologies on the threshold for clinically overt dementia. *Acta Neuropathologica, 134*(2), 171–186. https://doi.org/10.1007/s00401-017-1717-7

[3] McKeith, I. G., Boeve, B. F., Dickson, D. W., Halliday, G., Taylor, J.-P., Weintraub, D., Aarsland, D., Galvin, J., Attems, J., Ballard, C. G., Bayston, A., Beach, T. G., Blanc, F., Bohnen, N., Bonanni, L., Bras, J., Brundin, P., Burn, D., Chen-Plotkin, A., … Kosaka, K. (2017). Diagnosis and management of dementia with Lewy bodies: Fourth consensus report of the DLB Consortium. *Neurology, 89*(1), 88–100. https://doi.org/10.1212/WNL.0000000000004058

[4] Boyle, P. A., Yu, L., Leurgans, S. E., Wilson, R. S., Brookmeyer, R., Schneider, J. A., & Bennett, D. A. (2019). Attributable risk of Alzheimer's dementia attributed to age-related neuropathologies. *Annals of Neurology, 85*(1), 114–124. https://doi.org/10.1002/ana.25380

[5] Bennett, D. A., Buchman, A. S., Boyle, P. A., Barnes, L. L., Wilson, R. S., & Schneider, J. A. (2018). Religious Orders Study and Rush Memory and Aging Project. *Journal of Alzheimer's Disease, 64*(s1), S161–S189. https://doi.org/10.3233/JAD-179939

[6] Habib, N., Avraham-Davidi, I., Basu, A., Burks, T., Shekhar, K., Hofree, M., Choudhury, S. R., Aguet, F., Gelfand, E., Ardlie, K., Weitz, D. A., Rozenblatt-Rosen, O., Zhang, F., & Regev, A. (2017). Massively parallel single-nucleus RNA-seq with DroNc-seq. *Nature Methods, 14*(10), 955–958. https://doi.org/10.1038/nmeth.4407

[7] Lake, B. B., Chen, S., Sos, B. C., Fan, J., Kaeser, G. E., Yung, Y. C., Duong, T. E., Gao, D., Chun, J., Kharchenko, P. V., & Zhang, K. (2018). Integrative single-cell analysis of transcriptional and epigenetic states in the human adult brain. *Nature Biotechnology, 36*(1), 70–80. https://doi.org/10.1038/nbt.4038

[8] Grubman, A., Chew, G., Ouyang, J. F., Sun, G., Choo, X. Y., McLean, C., Simmons, R. K., Buckberry, S., Vargas-Landin, D. B., Poppe, D., Pflueger, J., Lister, R., Rackham, O. J. L., Petretto, E., & Polo, J. M. (2019). A single-cell atlas of entorhinal cortex from individuals with Alzheimer's disease reveals cell-type-specific gene expression regulation. *Nature Neuroscience, 22*(12), 2087–2097. https://doi.org/10.1038/s41593-019-0539-4

[9] Lau, S.-F., Cao, H., Fu, A. K. Y., & Ip, N. Y. (2020). Single-nucleus transcriptome analysis reveals dysregulation of angiogenic endothelial cells and neuroprotective glia in Alzheimer's disease. *Proceedings of the National Academy of Sciences, 117*(41), 25800–25809. https://doi.org/10.1073/pnas.2008762117

[10] Leng, K., Li, E., Eser, R., Piergies, A., Sit, R., Tan, M., Neff, N., Li, S. H., Rodriguez, R. D., Suemoto, C. K., Leite, R. E. P., Ehrenberg, A. J., Allen, I. E., Zaitlen, N., Seeley, W. W., Heinsen, H., Grinberg, L. T., & Kampmann, M. (2021). Molecular characterization of selectively vulnerable neurons in Alzheimer's disease. *Nature Neuroscience, 24*(2), 276–287. https://doi.org/10.1038/s41593-020-00764-7

[11] Mathys, H., Davila-Velderrain, J., Peng, Z., Gao, F., Mohammadi, S., Young, J. Z., Menon, M., He, L., Abdurrob, F., Jiang, X., Martorell, A. J., Ransohoff, R. M., Hafler, B. P., Bennett, D. A., Kellis, M., & Tsai, L.-

H. (2019). Single-cell transcriptomic analysis of Alzheimer's disease. *Nature, 570*(7761), 332–337. https://doi.org/10.1038/s41586-019-1195-2

[12] Soreq, L., Bird, H., Mohamed, W., & Hardy, J. (2023). Single-cell RNA sequencing analysis of human Alzheimer's disease brain samples reveals neuronal and glial specific cells differential expression. *PLOS ONE, 18*(2), Article e0277630. https://doi.org/10.1371/journal.pone.0277630

[13] Zhou, Y., Song, W. M., Andhey, P. S., Swain, A., Levy, T., Miller, K. R., Poliani, P. L., Cominelli, M., Grover, S., Gilfillan, S., Cella, M., Ulland, T. K., Zaitlen, N., Mathys, H., Peng, Z., Bennett, D. A., Schneider, J. A., Bales, K. R., Paul, S. M., … Colonna, M. (2020). Human and mouse single-nucleus transcriptomics reveal TREM2-dependent and TREM2-independent cellular responses in Alzheimer's disease. *Nature Medicine, 26*(1), 131–142. https://doi.org/10.1038/s41591-019-0695-9

[14] Habib, N., McCabe, C., Medina, S., Varshavsky, M., Kitsberg, D., Dvir-Szternfeld, R., Green, G., Dionne, D., Nguyen, L., Marshall, J. L., Chen, F., Zhang, F., Kaplan, T., Regev, A., & Schwartz, M. (2020). Disease-associated astrocytes in Alzheimer's disease and aging. *Nature Neuroscience, 23*(6), 701–706. https://doi.org/10.1038/s41593-020-0624-8

[15] Keren-Shaul, H., Spinrad, A., Weiner, A., Matcovitch-Natan, O., Dvir-Szternfeld, R., Ulland, T. K., David, E., Baruch, K., Lara-Astaiso, D., Toth, B., Itzkovitz, S., Colonna, M., Schwartz, M., & Amit, I. (2017). A unique microglia type associated with restricting development of Alzheimer's disease. *Cell, 169*(7), 1276–1290.e17. https://doi.org/10.1016/j.cell.2017.05.018

[16] Arvanitakis, Z., Leurgans, S. E., Barnes, L. L., Bennett, D. A., & Schneider, J. A. (2011). Microinfarct pathology, dementia, and cognitive systems. *Stroke, 42*(3), 722–727. https://doi.org/10.1161/STROKEAHA.110.595082

[17] Nelson, P. T., Dickson, D. W., Trojanowski, J. Q., Jack, C. R., Boyle, P. A., Arfanakis, K., Rademakers, R., Alafuzoff, I., Attems, J., Brayne, C., Coyle-Gilchrist, I. T. S., Chui, H. C., Fardo, D. W., Flanagan, M. E., Halliday, G., Hokkanen, S. R. K., Hunter, S., Jicha, G. A., Katsumata, Y., Kawas, C. H., Keene, C. D., Kovacs, G. G., Kukull, W. A., Levey, A. I., Makkinejad, N., Montine, T. J., Murayama, S., Murray, M. E., Nag, S., Rissman, R. A., Seeley, W. W., Sperling, R. A., White, C. L., Yu, L., & Schneider, J. A. (2019). Limbic-predominant age-related TDP-43 encephalopathy (LATE): Consensus working group report. *Brain, 142*(6), 1503–1527. https://doi.org/10.1093/brain/awz099

[18] Park, H., He, Y., He, Y., Adikari, S. H., Leong, Y. A., Wang, H., Yim, Y. S., Jones, K. R., & Han, M. H. (2023). Single-cell RNA-sequencing identifies disease-associated oligodendrocytes in male APPNL-G-F and 5XFAD mice and human Alzheimer's disease brains. *Nature Communications, 14*, Article 1532. https://doi.org/10.1038/s41467-023-36519-8

[19] Seattle Alzheimer's Disease Brain Cell Atlas. (n.d.). SEA-AD: Seattle Alzheimer's disease brain cell atlas. *Allen Institute Brain Map*. https://brain-map.org/consortia/sea-ad

[20] Deczkowska, A., Keren-Shaul, H., Weiner, A., Colonna, M., Schwartz, M., & Amit, I. (2018). Disease-associated microglia: A universal immune sensor of neurodegeneration. *Cell, 173*(5), 1073–1081. https://doi.org/10.1016/j.cell.2018.05.003

[21] Leng, F., & Edison, P. (2021). Neuroinflammation and microglial activation in Alzheimer disease: Where do we go from here? *Nature Reviews Neurology, 17*(3), 157–172. https://doi.org/10.1038/s41582-020-00435-y

[22] Blanchard, J. W., Akay, L. A., Davila-Velderrain, J., von Maydell, D., Mathys, H., Davidson, S. M., Effenberger, A., Chen, C.-Y., Maner-Smith, K., Hajjar, I., Ortlund, E. A., Bula, M., Agbas, E., Ng, A., Jiang, X., Kahn, M., Blanco-Duque, C., Lavoie, N., Liu, L., Reyes, R., Lin, Y.-T., Ko, T., R'Bibo, L., Ralvenius, W. T., Bennett, D. A., Cam, H. P., Kellis, M., Tsai, L.-H., & Yankner, B. A. (2022). APOE4 impairs myelination via cholesterol dysregulation in oligodendrocytes. *Nature, 611*(7937), 769–779. https://doi.org/10.1038/s41586-022-05439-w

[23] Quinn, T. P., Erb, I., Richardson, M. F., & Crowley, T. M. (2018). Understanding sequencing data as compositions: An outlook and review. *Bioinformatics, 34*(16), 2870–2878.

https://doi.org/10.1093/bioinformatics/bty175

[24] Gouwens, N. W., Sorensen, S. A., Berg, J., Lee, C., Jarsky, T., Ting, J., Sunkin, S. M., Feng, D., Anastassiou, C. A., Barkan, E., Bickley, K., Blesie, N., Braun, T., Brouner, K., Budzillo, A., Caldejon, S., Casper, T., Castelli, D., Chong, P., … Zeng, H. (2020). Integrated morphoelectric and transcriptomic classification of cortical GABAergic cells. *Cell, 183*(4), 935–953.e19. https://doi.org/10.1016/j.cell.2020.09.057

[25] Nation, D. A., Sweeney, M. D., Montagne, A., Sagare, A. P., D'Orazio, L. M., Pachicano, M., Sepehrband, F., Nelson, A. R., Buennagel, D. P., Harrington, M. G., Benzinger, T. L. S., Fagan, A. M., Ringman, J. M., Schneider, L. S., Morris, J. C., Chui, H. C., Law, M., Toga, A. W., & Zlokovic, B. V. (2019). Blood-brain barrier breakdown is an early biomarker of human cognitive dysfunction. *Nature Medicine, 25*(2), 270–276. https://doi.org/10.1038/s41591-018-0297-y

[26] Sweeney, M. D., Sagare, A. P., & Zlokovic, B. V. (2018). Blood-brain barrier breakdown in Alzheimer disease and other neurodegenerative disorders. *Nature Reviews Neurology, 14*(3), 133–150. https://doi.org/10.1038/nrneurol.2017.188

[27] Montagne, A., Nation, D. A., Sagare, A. P., Barisano, G., Sweeney, M. D., Chakhoyan, A., Pachicano, M., Joe, E., Nelson, A. R., D'Orazio, L. M., Buennagel, D. P., Harrington, M. G., Benzinger, T. L. S., Fagan, A. M., Ringman, J. M., Schneider, L. S., Morris, J. C., Reiman, E. M., Caselli, R. J., Chui, H. C., Tcw, J., Chen, Y., Pa, J., Conti, P. S., Law, M., Toga, A. W., & Zlokovic, B. V. (2020). APOE4 leads to blood-brain barrier dysfunction predicting cognitive decline. *Nature, 581*(7806), 71–76. https://doi.org/10.1038/s41586-020-2247-3

[28] Trejo-Lopez, J. A., Yachnis, A. T., & Prokop, S. (2022). Neuropathology of Alzheimer's disease. *Neurotherapeutics, 19*(1), 173–185. https://doi.org/10.1007/s13311-021-01146-y

[29] Jack, C. R., Jr., Andrews, J. S., Beach, T. G., Buracchio, T., Dunn, B., Graf, A., Hansson, O., Ho, C., Jagust, W., McDade, E., Molinuevo, J. L., Nelson, P. T., Rafii, M. S., Scheltens, P., Siemers, E., Snyder, H. M., Sperling, R., & Teunissen, C. E. (2024). Revised criteria for diagnosis and staging of Alzheimer's disease. *Alzheimer's & Dementia, 20*(8), 5143–5169. https://doi.org/10.1002/alz.13859

[30] Highet, B., Parker, R., Faull, R. L. M., Curtis, M. A., & Ryan, B. (2021). RNA quality in post-mortem human brain tissue is affected by Alzheimer's disease. *Frontiers in Molecular Neuroscience, 14*, Article 780352. https://doi.org/10.3389/fnmol.2021.780352

[31] Tian, J., Lee, A. W., & Teich, A. F. (2025). An analysis of RNA quality metrics in human brain tissue. *Journal of Neuropathology & Experimental Neurology, 84*(3), 236–243. https://doi.org/10.1093/jnen/nlae132

Appendix

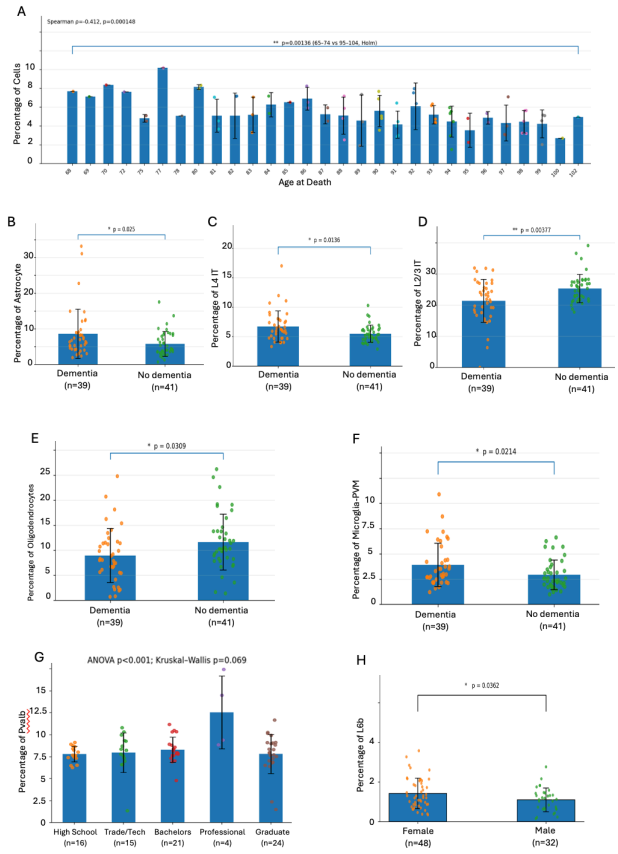

Figure A1. Demographic and dementia-status associations with cell-type proportions. (A) Bar-and-dot plot showing the plotted percentage measure across age at death. The x-axis represents age at death in years, and the y-axis represents percentage of cells. Bars show the mean for each age, colored points represent individual donors, and error bars show standard deviations. The Spearman rank-correlation coefficient and corresponding *p* value are displayed above the panel. The horizontal bracket marks the Holm-adjusted comparison between donors aged 65–74 years and those aged 95–104 years. (B–F) Bar-and-dot plots comparing donors with dementia ($n = 39$; orange points) and without dementia ($n = 41$; green points). The x-axis represents dementia status, and the y-axis represents donor-level percentages of astrocytes (B), L4 intratelencephalic neurons (L4 IT; C), L2/3 intratelencephalic neurons (L2/3 IT; D), oligodendrocytes (E), and microglia/perivascular macrophages (microglia-PVM; F). Blue bars show group means, points show individual donors, and error bars show standard deviations. Horizontal brackets and exact *p* values indicate two-group comparisons. (G) Bar-and-dot plot of Pvalb interneuron percentage across education categories: high school ($n = 16$), trade/technical school ($n = 15$), bachelor's degree ($n = 21$), professional degree ($n = 4$), and graduate degree ($n = 24$). The x-axis represents education category, and the y-axis represents Pvalb percentage. One-way analysis of variance (ANOVA) and Kruskal–Wallis *p* values are reported above the panel. (H) Bar-and-dot plot comparing L6b percentage between female ($n = 48$; orange points) and male ($n = 32$; green points) donors. The x-axis represents sex, and the y-axis represents L6b percentage. Blue bars show group means, points show individual donors, and error bars show standard deviations. The bracket and exact *p* value indicate the two-group comparison. ** and * indicate statistical significance at the 1% and 5% levels respectively.

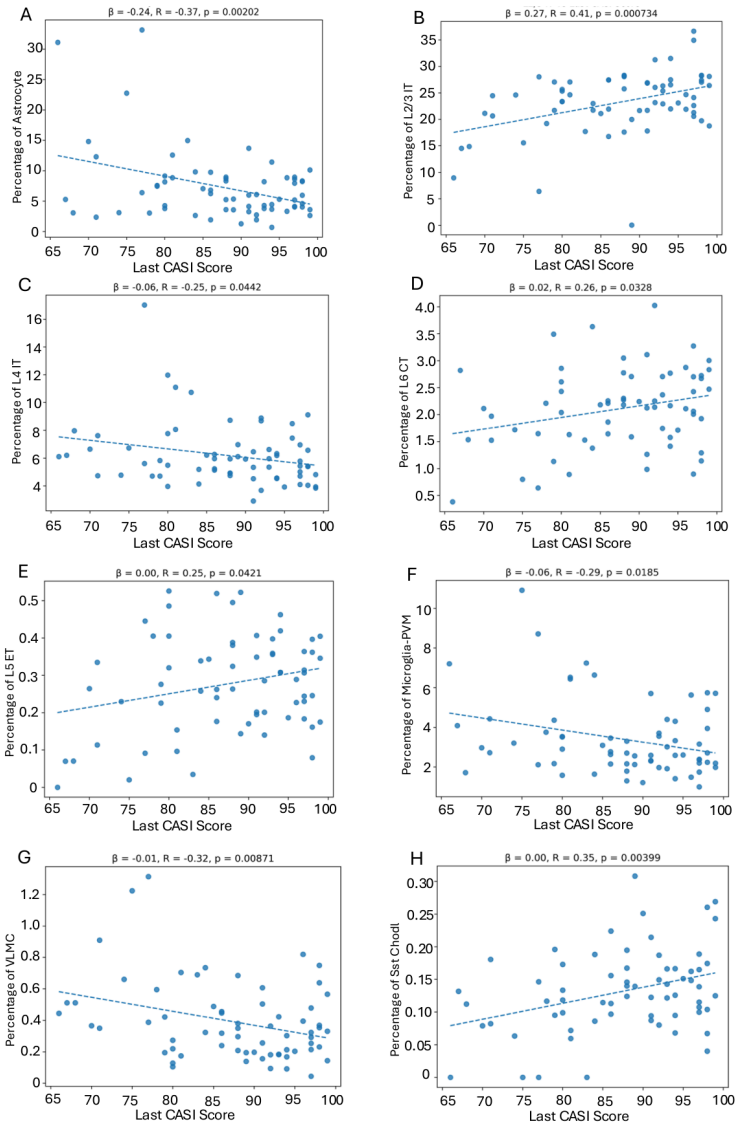

Figure A2. Associations between last CASI score and selected neuronal, glial, immune, and vascular-associated cell-type proportions. Panels show donor-level scatterplots relating the last available Cognitive Abilities Screening Instrument (CASI) score to cell-type percentages. The x-axis in all panels represents the last CASI score, with higher values indicating better cognitive performance. The y-axis represents the percentage of astrocytes (A), L2/3 intratelencephalic neurons (L2/3 IT; B), L4 intratelencephalic neurons (L4 IT; C), L6 corticothalamic neurons (L6 CT; D), L5 extratelencephalic neurons (L5 ET; E), microglia/perivascular macrophages (microglia-PVM; F), vascular leptomeningeal cells (VLMCs; G), and Sst Chodl interneurons (H). Each blue point represents one donor with nonmissing CASI and cell-type data, and the dashed line represents the fitted linear regression line. The regression coefficient (β), Pearson correlation coefficient (R), and exact p value are reported above each panel. Analyses used available-case data from the full cohort of 80 donors.

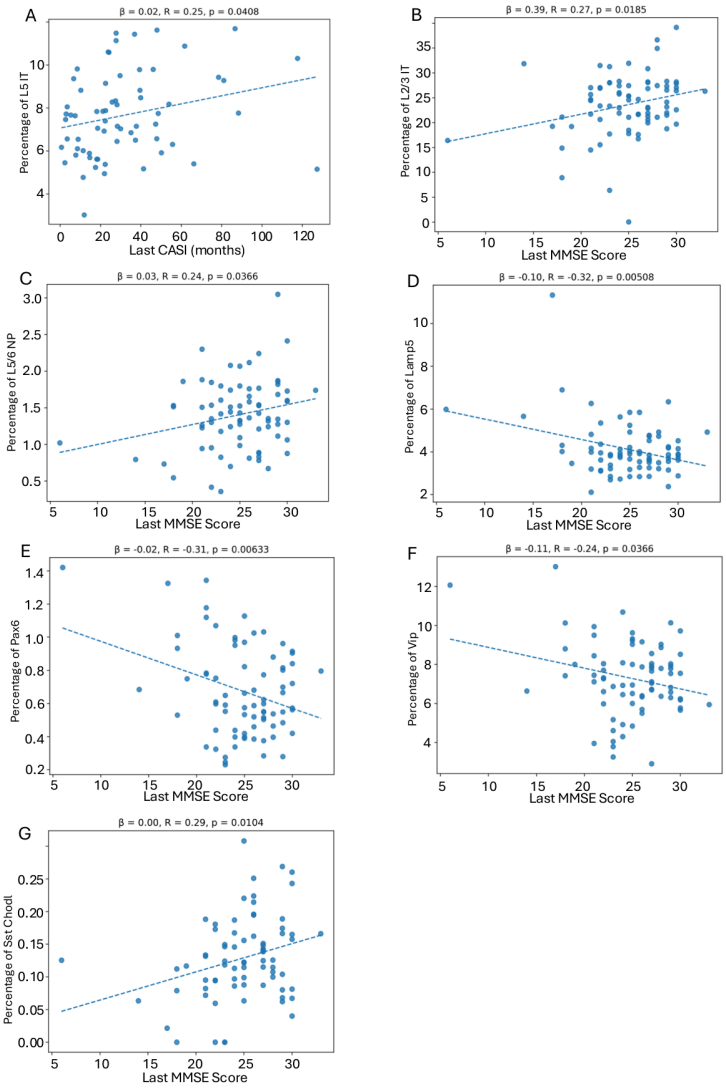

Figure A3. Associations of the interval from cognitive assessment to death and last MMSE score with selected neuronal cell-type proportions. (A) Scatterplot showing the association between the number of months from the last CASI assessment to death and the percentage of L5 intratelencephalic neurons (L5 IT). The x-axis represents the last-CASI-to-death interval in months, and the y-axis represents L5 IT percentage. (B–G) Scatterplots showing donor-level cell-type percentages in relation to the last available Mini-Mental State Examination (MMSE) score. The x-axis represents the last MMSE score, and the y-axis represents the percentage of L2/3 intratelencephalic neurons (L2/3 IT; B), L5/6 near-projecting neurons (L5/6 NP; C), Lamp5 interneurons (D), Pax6 interneurons (E), Vip interneurons (F), and Sst Chodl interneurons (G). In all panels, each blue point represents one donor with nonmissing data, and the dashed line represents the fitted linear regression line. The regression coefficient (β), Pearson correlation coefficient (R), and exact p value are reported above each panel. Analyses used available-case data from the full cohort of 80 donors.

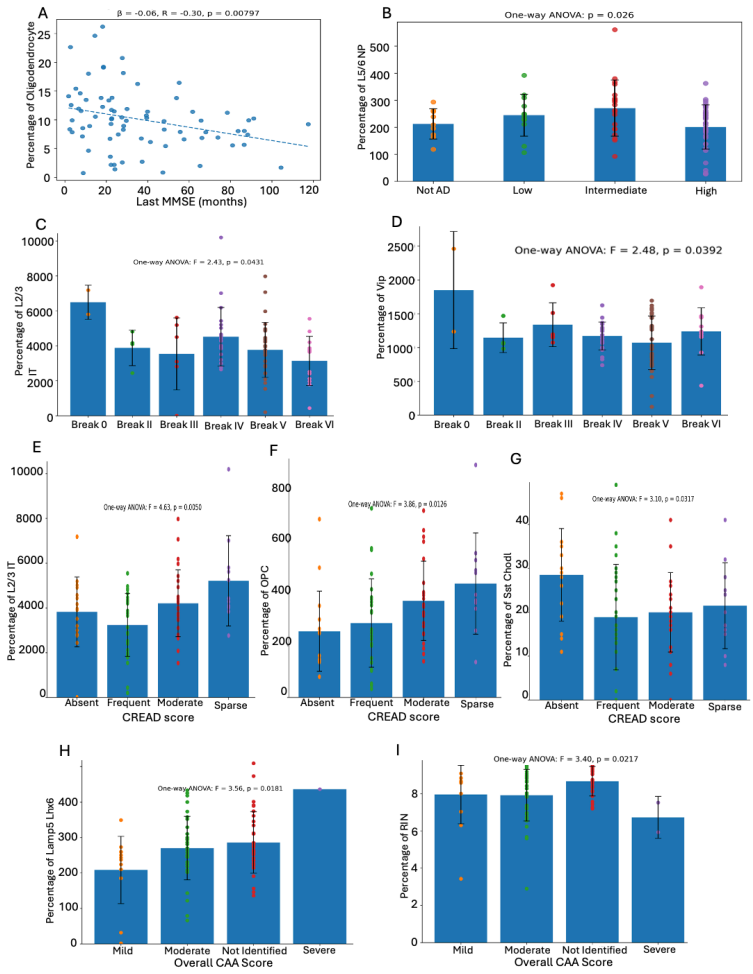

Figure A4. Associations of cognitive-assessment interval, Alzheimer's disease neuropathologic measures, cerebral amyloid angiopathy, and RNA integrity with cell-type measures. (A) Scatterplot showing oligodendrocyte percentage in relation to the number of months from the last MMSE assessment to death. The x-axis represents the last-MMSE-to-death interval in months, and the y-axis represents oligodendrocyte percentage. Each point represents one donor, the dashed line represents the fitted linear regression line, and β, R, and the exact p value are displayed above the panel. (B) Bar-and-dot plot of L5/6 near-projecting neuron (L5/6 NP) abundance across Alzheimer's disease neuropathologic classification categories: not AD, low, intermediate, and high. (C–D) Bar-and-dot plots of L2/3 intratelencephalic neuron (L2/3 IT; C) and Vip interneuron (D) abundance across Braak stages. (E–G) Bar-and-dot plots of L2/3 IT (E), oligodendrocyte precursor cell (OPC; F), and Sst Chodl (G) abundance across CERAD neuritic plaque-score categories. (H–I) Bar-and-dot plots of Lamp5 Lhx6 abundance (H) and RNA integrity number (RIN; I) across overall cerebral amyloid angiopathy (CAA) categories. In Panels B–I, the x-axis represents the corresponding neuropathologic category and the y-axis represents the plotted cell-type measure or RIN value. Blue bars show group means, colored points show individual donors, and error bars show standard deviations. Multigroup comparisons were evaluated using one-way ANOVA, with the omnibus F statistic when shown and the exact p value displayed above each panel. Analyses used available-case data from the full cohort of 80 donors.

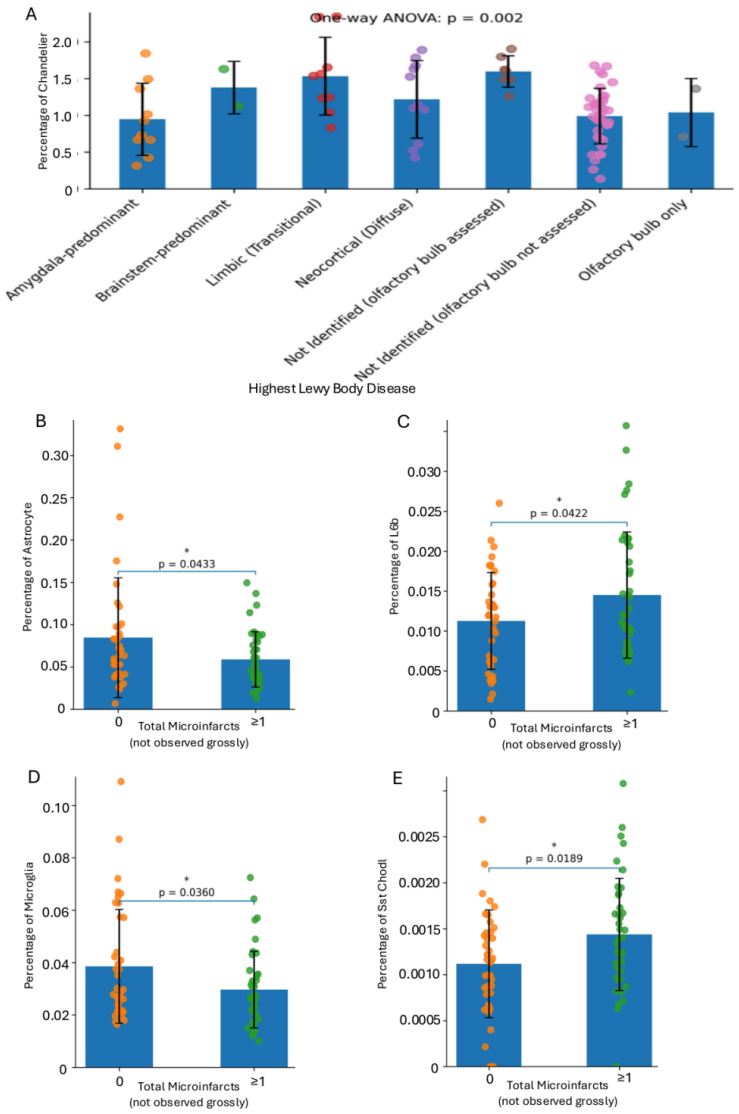

Figure A5. Associations of Lewy body disease and microinfarcts not observed grossly with chandelier, astrocyte, L6b, microglial, and Sst Chodl proportions. (A) Bar-and-dot plot showing chandelier-cell percentage across the highest recorded Lewy body disease categories: amygdala-predominant, brainstem-predominant, limbic (transitional), neocortical (diffuse), not identified with olfactory bulb assessed, not identified with olfactory bulb not assessed, and olfactory-bulb-only disease. The x-axis represents Lewy body disease classification, and the y-axis represents chandelier-cell percentage. Blue bars show category means, colored points represent individual donors, error bars show standard deviations, and the omnibus *p* value is displayed above the panel. (B–E) Bar-and-dot plots comparing donors with no microinfarcts and donors with one or more microinfarcts not observed grossly. The x-axis represents microinfarct status, and the y-axis represents astrocyte (B), L6b (C), microglial (D), and Sst Chodl (E) percentage. Orange points represent donors with no microinfarcts, green points represent donors with at least one microinfarct, blue bars show group means, and error bars show standard deviations. Horizontal brackets and exact *p* values indicate two-group comparisons. * indicates statistical significance at the 5% level respectively. Analyses used available-case data from the full cohort of 80 donors.

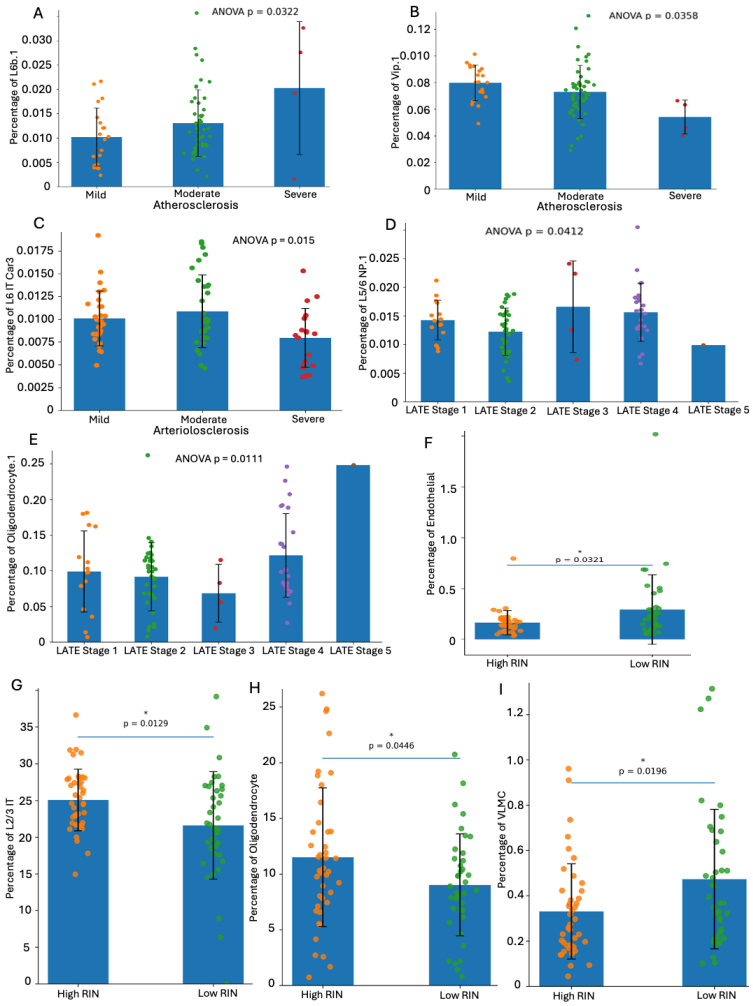

Figure A6. Associations of vascular pathology, LATE stage, and RNA integrity with selected neuronal, glial, endothelial, and vascular-associated cell-type proportions. (A–B) Bar-and-dot plots showing L6b.1 (A) and Vip.1 (B) percentages across mild, moderate, and severe atherosclerosis categories. (C) Bar-and-dot plot showing L6 IT Car3 percentage across mild, moderate, and severe arteriolosclerosis categories. (D–E) Bar-and-dot plots showing L5/6 NP.1 (D) and oligodendrocyte.1 (E) percentages across Limbic-predominant Age-related TDP-43 Encephalopathy (LATE) stages 1–5. For Panels A–E, the x-axis represents pathology severity or stage, the y-axis represents the corresponding cell-type percentage, blue bars show group means, colored points represent individual donors, and error bars show standard deviations. Multigroup comparisons were evaluated using one-way ANOVA, and the omnibus *p* value is displayed above each panel. (F–I) Bar-and-dot plots comparing donors categorized as having high or low RNA Integrity Number (RIN). The x-axis represents RIN group, and the y-axis represents endothelial-cell (F), L2/3 intratelencephalic neuron (L2/3 IT; G), oligodendrocyte (H), and vascular leptomeningeal cell (VLMC; I) percentage. Orange points represent high-RIN donors, green points represent low-RIN donors, blue bars show group means, and error bars show standard deviations. Horizontal brackets and exact *p* values indicate two-group comparisons. * indicates statistical significance at the 5% level respectively. Analyses used available-case data from the full cohort of 80 donors.